Recoupling Dipolar Interactions with Multiple I = 1 Quadrupolar Nuclei: A $^{11}B\{^{6}Li\}$ and $^{31}P\{^{6}Li\}$ Rotational Echo Double Resonance Study of Lithium Borophosphate Glasses.

Lena Marie Funke,[a] Henrik Bradtmüller,[a] and Hellmut Eckert[a,b,*]

[a]Institut für Physikalische Chemie
Westfälische Wilhelms-Universität Münster
Corrensstraße 30
D 48149, Münster, Germany

[b]Instituto de Física em São Carlos
Universidade de São Paulo
CEP 369, São Carlos 13566-590

Dedicated to Professor Jean-Paul Amoureux on the occasion of his 70th birthday

Abstract

The case of rotational echo double resonance (REDOR) experiments on the observe nuclei ^{11}B and ^{31}P interacting with multiple $I = 1$ quadrupolar nuclei is analyzed in detail by SIMPSON simulations and experimental studies. The simulations define the region within the parameter space spanned by nutation frequency, quadrupolar coupling constant and spinning frequency where the parabolic analysis of the initial REDOR curve in terms of dipolar second moments has validity. The predictions are tested by experimental studies on the crystalline model compounds lithium diborate and lithium pyrophosphate, which are subsequently extended to measure dipolar second moments $M_2(^{11}B\{^{6}Li\})$ and $M_2(^{31}P\{^{6}Li\})$ in three borophosphate glasses. The data indicate that the lithium cations interact significantly more strongly with the phosphate than with the borate species, despite the formally anionic character of four-coordinate boron and the formally neutral character of the formally neutral ultraphosphate ($P^{(3)}$) units to which they are linked.

Key words: REDOR, quadrupolar interactions, borophosphate glasses, dipolar coupling

*corresponding author, E-mail: eckerth@uni-muenster.de

Introduction

Rotational echo double resonance (REDOR) experiments in which the magnetic dipole-dipole interactions between an observe nucleus *S* and another nucleus *I* are re-coupled enjoy widespread popularity in different fields of scientific endeavor [1-5]. While initially conceived (and predominantly used) for distance measurements between pairs of spin-1/2 nuclei in doubly labeled biological solids [2,3,6], during the past 15 years the scope of applications has broadened considerably, including disordered crystals, glasses, and inorganic-organic nanocomposites [4,5]. Most of the latter applications involve the measurement of multi-spin interactions comprising different numbers of interacting nuclei over widely spread-out distance ranges. As has been previously shown by us, the dipolar coupling within such ill-defined and distributed spin systems are described most effectively by average second moments, which can be measured rather conveniently from the initial data range ($\Delta S/S_0 \leq$ 0.2 to 0.3) of the REDOR curve. [6]. Additional inherent complications concerned with REDOR measurements of inorganic systems arise when quadrupolar nuclei (nuclei having spin quantum numbers larger than 1/2) are involved. One aspect is the occurrence of the dephaser nuclei in different Zeeman states, which produce *S*-nucleus dephasing of different magnitudes. A further complication arises from strong first-order quadrupolar splittings encountered with half-integer quadrupolar nuclei. In this case the magnitude of the REDOR effect of the observe nucleus is compromised by off-resonance irradiation of those dephaser nuclei that are in the non-central Zeeman states. A number of experimental strategies, among them the RESPDOR technique [7] have been designed to deal with such complications [7-12]. The less-common case, namely that of dipolar recoupling to nuclei with integral spin quantum numbers has been discussed for spin-1/2- spin-1 pairs by various authors [12,13], however, to the best of our knowledge no application to disordered inorganic multiple-spin systems can be found in the literature. Such situations may occur, for example, in glasses enriched with the ^{6}Li isotope (I = 1), which is frequently introduced as a convenient probe of chemical bonding and ion dynamics in solid electrolyte materials [14-16].

In the present contribution, we have introduced this isotope with the objective of measuring the magnetic dipole-dipole interactions between the network-modifying lithium ions and the network former species boron and phosphorus in lithium borophosphate glasses by rotational echo double resonance. The glasses under consideration are characterized by strong network former mixing effects on various bulk properties, indicating the formation of new medium-range structures not represented in the binary systems Li_2O-B_2O_3 and Li_2O-P_2O_5. Standard ^{11}B

and ^{31}P MAS-NMR spectra, supported by ^{11}B{^{31}P} rotational echo double resonance reveal the distinct preference of the boron atoms to occur in the four-coordinated state ($B^{(4)}$ units) having the maximum number of B-O-P linkages that is possible for a given glass composition. $(B(OP)_4$ units. In the borophosphate glass literature these are denoted as $B^{(4)}_{4P}$ species, where the superscript denotes the number of bridging oxygen atoms linked to other network former species, whereas the subscript denotes the number of B-O-P linkages [17]. Even though the $B^{(4)}_{4P}$ species have a negative formal charge, bond valence considerations suggest that these anionic charges are actually dispersed onto the non-bridging oxygen atoms of the phosphate species to which these $B^{(4)}$ units are linked [17]. Indeed in sodium borophosphate glasses this view has been supported by a comparative analysis of ^{31}P{^{23}Na} and ^{11}B{^{23}Na} magnetic dipole interactions [18]. To examine the question whether this behavior is a general feature of alkali borophosphate glasses and independently test the conclusions of reference [18] on a different system, we decided to carry out an analogous double resonance study of lithium borophosphate glasses. At natural abundance, 92.4 % of the lithium atoms contain the nuclear isotope ^{7}Li, but the close proximity of its nuclear Zeeman frequency to those of ^{11}B and ^{31}P requires special hardware set up for double resonance studies [19], and makes the quantification of dipolar interactions rather difficult. As an alternative we have turned to the study of ^{6}Li enriched glasses, which is more straightforward to carry out experimentally, but requires appropriate attention to the effects of dipolar interactions to the quadrupolar spin-1 nuclei. In the present contribution we report our simulations and experimental results concerning the measurement of heteronuclear dipolar second moments characterizing the interaction of ^{11}B and ^{31}P with multiple ^{6}Li spins ($I = 1$) in lithium borophosphate glasses and the crystalline model compounds $Li_2B_4O_7$ and $Li_4P_2O_7$.

Experimental

Sample Preparation and Characterization. Table 1 summarizes the compositions and physical properties of the glasses under investigation. The starting materials, anhydrous Li_2CO_3 (Sigma Aldrich, 95 atom% ^{6}Li) and $NH_4H_2PO_4$ (Acros, 99.9%) were pre-dried for 48 h at 120 °C. B_2O_3 (Acros, 99%) was heated for 2 h at 900 °C in a platinum crucible and the resulting melt was quenched to form a glass. It was immediately stored in an argon filled box and powdered only immediately before glass preparation. 1-3 g batches of the mixtures (see Tab. 2) were degassed and melted in a platinum crucible inside a Thermoconcept muffle furnace at 1000-1200 °C for 15 min. Melts were quenched by placing the crucible onto a copper plate held

at room temperature. To limit exposure to ambient moisture and ensure sample quality over a long period of time, glass samples were stored in an argon filled glove box. All glasses were found to be homogenous and transparent. Excess mass losses were less than or equal to 3 %. Thermal analyses were carried out with a Netzsch Phönix differential scanning calorimeter using a heating rate of 10 K min^{-1} and glass transition temperatures were determined from the onset region of the observed thermal event by the tangent intersection method. A LabRAM HR Raman microscope spectrometer from Jobin Yvon Horiba was used to collect the Raman spectra from smooth sample regions. The spectra were recorded using a 532 nm laser focused with a 50×objective, a 1800 1⁄mm grating and a CCD-detector operated at an acquisition time of 10 s. 50 to 100 scans were averaged to enhance the signal-to-noise ratio. The ^{6}Li enriched model compounds $^{6}Li_2B_4O_7$ and $^{6}Li_4P_2O_7$ were obtained by crystallization of the corresponding stoichiometric glasses, at annealing temperatures and annealing times of 550 °C, 20 h and 830 °C, respectively, for 10 min prior to slow cooling at a rate of 13 K h^{-1}. The phase purity of these crystalline compounds was ascertained by X-ray powder diffraction, using a FR 552 Guinier-camera from Enraf-Nonius.

Table 1: Glass Compositions and glass transition temperatures, T_g, obtained in the present study:

	Composition Li_2O:B_2O_3:P_2O_5	Mole% Li_2O	Mole% B_2O_3	Mole% P_2O_5	T_g/K (±5K)
B	1.0:1.0:2.0	25.0	25.0	50.0	714
C	1.0:0.5:1.5	33.3	16.7	50.0	662
D	1.0:2.0:0.0	33.3	66.7	-	764

Solid State NMR. All experiments were conducted at room temperature on a Bruker-Avance-III 300 MHz spectrometer, a Bruker-Avance-DSX-400 spectrometer and a Bruker-Avance-DSX-500 spectrometer, equipped with fast MAS capabilities. To minimize radio frequency amplitude inhomogeneity all the REDOR experiments were conducted with rotors that were only filled in the center 1/3 of their total volumes. The ^{11}B-MAS-NMR spectra were recorded at 7.05 and 11.74 T in 4 mm MAS probes operated at a spinning frequency of ν_r = 13.0 kHz and pulse lengths of 1.0 μs were used at a nutation frequency of 26 kHz on a liquid sample (22.5° flip angle). For the three-coordinate ^{11}B nuclei this corresponded to selective excitation conditions. To ensure complete relaxation, signal averaging required recycle delays of 5 s. The ^{31}P-MAS-NMR spectra were recorded at 7.05 T using a 2.5 mm MAS probe operated at a spinning frequency 28.0 kHz. Recycle delays of 1000 s were required. ^{7}Li single pulse experiments were conducted at 9.4 T (155.5 MHz), using a 4 mm MAS probe operated at a

spinning speed of 2.5 kHz. Short excitation pulses of 0.5 μs were used and recycle delays were set to 1-20 s. The Fourier transformed phased signals were analyzed using the Dmfit 2011 program package [20]. The specific measurement conditions selected for the various heteronuclear *I* - *S* double resonance experiments are summarized in Table 2. They were conducted with a saturation comb ensuring reproducible initial conditions. Lithium pyrophosphate ($Li_4P_2O_7$) and lithium diborate ($Li_2B_4O_7$) were used as reference and calibration materials. All the REDOR experiments used the standard sequence of Gullion and Schaefer [1] using XY-4 phase cycles [21] on the recoupling π-pulses. In the case of the $^{11}B\{^6Li\}$ REDOR studies, two separate series of experiments were done, optimizing the respective 180° pulse conditions for the observation of the rotorsynchronized spin echoes arising from the three- and four-coordinate ^{11}B nuclei. While the three coordinate boron units were observed in the limit of selective excitation of the m = ½ <-> m = -1/2 transition, this was not the case for the four-coordinate boron units. Simulations of $^{31}P\{^6Li\}$ REDOR experiments were conducted on two-spin systems, considering the effects of nutation frequency, MAS rotor frequency, ^6Li nuclear quadrupolar interaction strength, as well as heterodipolar interaction strength, using the SIMPSON program [22].

Table 2: Measurement conditions for the double resonance experiments conducted in the present study.

Experiment	B_0 / T	ν_r / kHz	t_p^c (π) / μs (obs.)	t_p^c (π) / μs (non-obs.)	D_1^d / s
$^{11}B\{^6Li\}$ REDOR	9.4	13.0	6.2[a],4.7[b]	24.4	5-10
$^{31}P\{^6Li\}$ REDOR	11.7	10.5-14.0	11.7	28.3-37.0	240

[a]for four-coordinate boron, [b]for three-coordinate boron, [c]pulse length, [d]relaxation delay

Results and Discussion.

$^{31}P\{^6Li\}$ REDOR simulations.

As mentioned in the Introduction, the REDOR curves of heteronuclear *S*{*I*} spin systems are significantly influenced by the quadrupolar and spin-1 character of the dephaser nuclei. Figure 1 shows simulations of REDOR curves for $^{31}P\{^6Li\}$ two-spin systems under systematic variation of the experimental conditions defined by the parameter space comprised of the nutation frequency, the quadrupolar coupling constant and the spinning frequency. In these simulations a typical $^{31}P\cdots^6Li$ internuclear distance of 2.7 Å was used, and the electric field

gradient asymmetry parameter was set to 0.5 in the absence of experimental information. Simulations were carried out with 22 gamma-angles and 678 crystallite orientations. Upon further increase of these parameters no further change was noted. As expected, the simulations manifest the qualitatively intuitive prediction that those *S* nuclei interacting with an *I* nucleus that happens to be in its $m_I = 0$ Zeeman state remain uncoupled because those *I* nuclei produce zero magnetic field component along the direction of quantization [13]. On the other hand, those ^{6}Li nuclei that are in their $m = \pm 1$ orientation states contribute equally to dephasing, as the absolute values of their corresponding *z*-components are equal. Figures 1a-c show the effect of the ^{6}Li nuclear electric quadrupolar coupling strength at three different ^{6}Li nutation frequencies (16, 43, and 150 kHz) upon the ^{31}P{^{6}Li} REDOR curves, for a typical spinning speed of 13.0 kHz. For REDOR studies involving ^{11}B or ^{31}P observe-nuclei at magnetic field strengths in the 5-10 T range, such a spinning rate is usually sufficient for minimizing the intensities of spinning sidebands due to the chemical shift anisotropy (^{31}P) and for producing undistorted MAS-NMR lineshapes governed by second-order quadrupolar effects (^{11}B). Note that for each set of simulations the $\Delta S/S_0$ difference signals tend to converge upon a common parabolic curve at sufficiently short dipolar mixing times. In this limit the REDOR response effected by dipolar recoupling of the observed spins with a nucleus of spin *I* is approximated by the expression [10]

$$\frac{\Delta S}{S_0} = \frac{1}{2I+1}\left(\sum_{m=-I}^{I}(2m)^2\right)\frac{1}{\pi^2(I+1)I}(NT_r)^2 M_2, \qquad (1)$$

which for $I = 1$ turns into

$$\frac{\Delta S}{S_0} = \frac{4}{3\pi^2}(NT_R)^2 M_{2IS}. \qquad (2)$$

By fitting parabolae to the simulated curves over the appropriate data range, we find that for the particular dipolar coupling strength considered here the parabolic approximation within the typical data range of $\Delta S/S_0 \leq 0.2$ remains valid as long as $\nu_1 \geq 10\ C_Q$, and may still be usable with suitable calibration if $C_Q(^6\text{Li})$ lies within the range $5\ C_Q \leq \nu_1 \leq 10\ C_Q$ at this particular spinning frequency. The need for this calibration factor arises because the conditions of adiabaticity ($\nu_1^2 >> C_Q \times \nu_r$) and infinitely short π pulses compared to the rotor period are no longer fulfilled. Alternatively, for this condition, a more restricted data range $\Delta S/S_0 \leq 0.1$ may be used to analyse the data according to eq. (2) without the need for calibration. For nutation

frequencies that are lower than 5 C_Q the parabolic approximation becomes essentially unusable. While in principle a more favourable situation may be achieved by applying slower spinning rates (data not shown) this is not truly a good option in the present application, as the spinning sideband intensities would become too intense, complicating the REDOR analysis.

Experimental validation

To validate the ^{31}P{^{6}Li} and ^{11}B{^{6}Li} REDOR method for the conditions applied in the present work, the experimental values for M_{2IS} (S = ^{11}B or ^{31}P, I = ^{6}Li) need to be compared to the corresponding values calculated from the van Vleck equation [23],

$$M_{2IS} = \frac{4}{15}\left(\frac{\mu_o}{4\pi}\right)^2 I(I+1)\gamma_I^2\gamma_S^2\hbar^2\sum_I r_{IS}^{-6} \qquad (3)$$

To this end, the calibration factors to be used (if needed) in connection with eq. (2) need to be determined, which requires experimental values for the ^{6}Li quadrupolar coupling constants. Unfortunately, the latter are difficult to measure with accuracy by direct ^{6}Li observation [24,25]. Therefore, we measured the ^{7}Li quadrupolar coupling constants from satellite transition (SATRAS) NMR and converted them to values for ^{6}Li, considering the ratio of the nuclear electric quadrupole moments Q(^{6}Li)/Q(^{7}Li) of 1/49.6 [26].

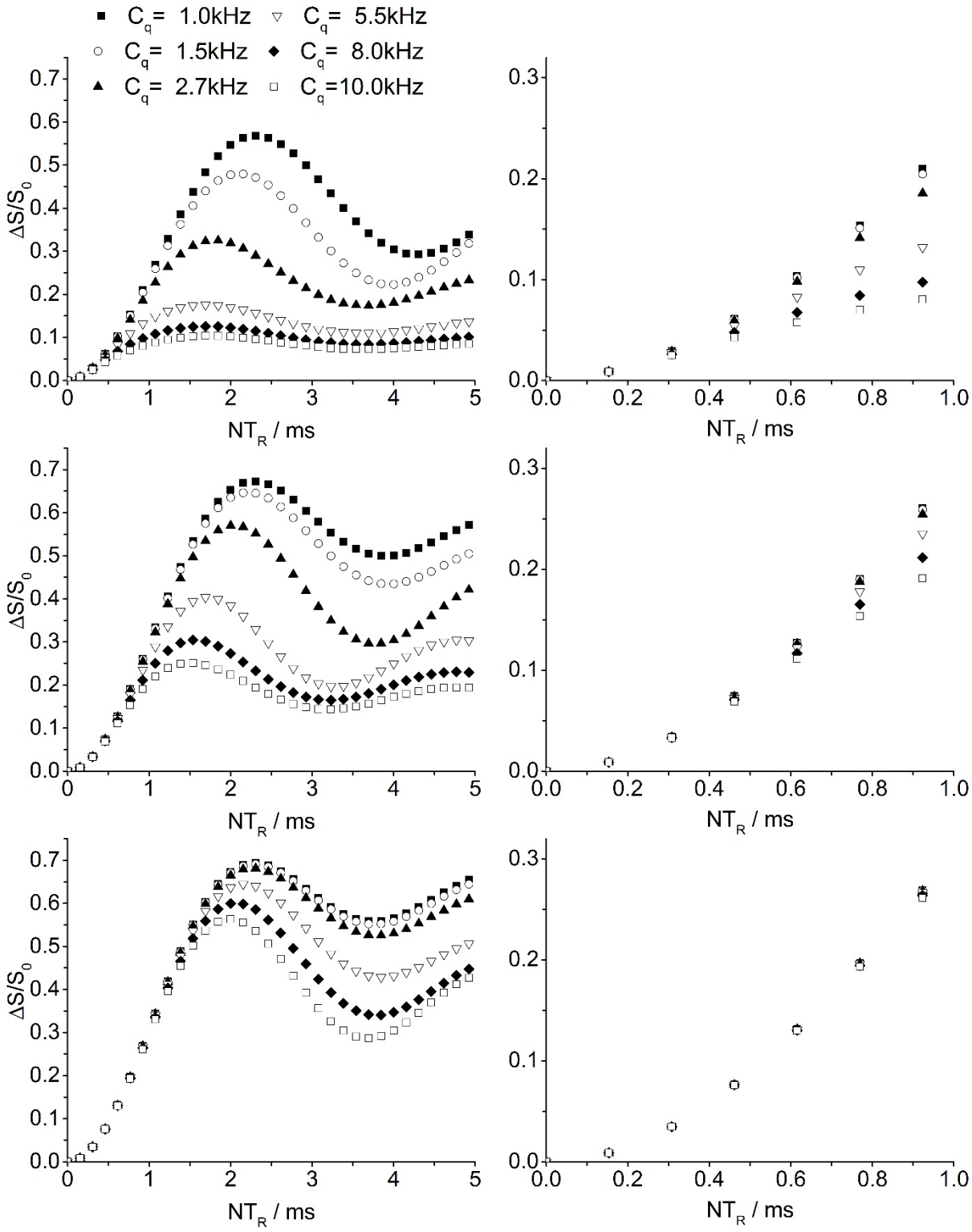

Figure 1: Simulated $^{31}P\{^{6}Li\}$ Left side: REDOR curves for a two-spin system with a distance of 2.7 Å at three different ^{6}Li nutation frequencies. Right side: simulated behavior at short evolution times illustrating the parabolic dependence at short evolution times in the initial data range $\Delta S/S_0 \leq 0.2$. From top to bottom: ^{6}Li nutation frequencies of 16, 43, and 150 kHz.

Figure 2 shows the ^{7}Li MAS-NMR results. For spin-3/2 nuclei the nuclear electric quadrupole coupling constant is equal to the total span of the spinning sideband patterns observed for the two $|m| = 3/2 \leftrightarrow |m| = 1/2$ single-quantum ("satellite") transitions [27]. We observe values of $C_Q = 155 \pm 5$ kHz for $Li_4P_2O_7$, and an average value of 170 ± 30 kHz for the three glasses. The larger uncertainty in the glasses reflects the presence of a distribution of nuclear electric quadrupole coupling constants, manifesting itself in a very gradual decrease of the spinning sideband intensities in the regions of the outermost spectral wings at the highest and lowest frequencies. Finally, the ^{7}Li quadrupole coupling constant and electric field gradient asymmetry parameter of crystalline lithium diborate are known to be 104.5 kHz and $\eta = 0.65$, as measured from previous single-crystal work [28,29]. From these data we can estimate the ^{6}Li nuclear electric quadrupole coupling constants to be 2.0 kHz, 3.0 kHz, and 3.5 kHz for $Li_2B_4O_7$, $Li_4P_2O_7$, and the glassy samples, respectively.

Figure 3 shows two-spin SIMPSON simulations of ^{31}P{^{6}Li} REDOR curves and of ^{11}B{^{6}Li} REDOR curves based on the experimental ^{6}Li nuclear electric quadrupole coupling constants, using exactly those pulse lengths, nutation frequencies and spinning speeds that were applied in the experimental study of each sample. These simulations were done to test (in view of the results shown in Figure 1) whether and to which extent a parabolic analysis of REDOR data within the data range $\Delta S/S_0 \leq 0.2$ will still reproduce the correct M_2 value under the actual conditions of the experimental measurement. In the case of the crystalline compounds $Li_2B_4O_7$ and $Li_4P_2O_7$, the effective internuclear distances used for the purpose of these test simulations are deduced from the theoretical M_2 values available via eq.(3) from crystallographic information [30,31]. Clearly, under the experimental conditions chosen, we are in a regime where the parabolic analysis is still applicable, however, the results show that fitting a parabola to the REDOR data range $\Delta S/S_0 \leq 0.2$ requires a calibration factor for reproducing the correct M_2 value. As indicated by Table 5, this simulated calibration factor (f_{sim}), determined by fitting a parabola to the simulated curves of Figure 3 within the data range $\Delta S/S_0 \leq 0.2$ is in very good agreement with the one (f_{exp}) determined experimentally, by comparing the raw experimental M_2 value obtained via application of eq. (2) to the REDOR data (M_{2raw}) with the theoretical one calculated via eq. (3). While for the model compounds the procedure is thus shown to work well, its validity has to be also examined for the glasses, in which the dipolar coupling is substantially weaker. To this end, Figure 3 includes analogous simulations, where the strength of the magnetic dipole coupling has been decreased to values of $0.3\times M_2$ and $0.1\times M_2$. As illustrated in Figure 3, the calibration factors turn out to be substantially different for these cases, their values decreasing with decreasing magnetic dipole-dipole coupling strengths. These

results indicate that under the experimental conditions used for the present study (non-adiabatic conditions, relatively long π pulses), the calibration factors determined for the crystalline model compounds are not directly applicable to the glasses. This fact has to be kept in mind with regard to the analysis of the experimental REDOR data on the glasses via eq. (2) as discussed below.

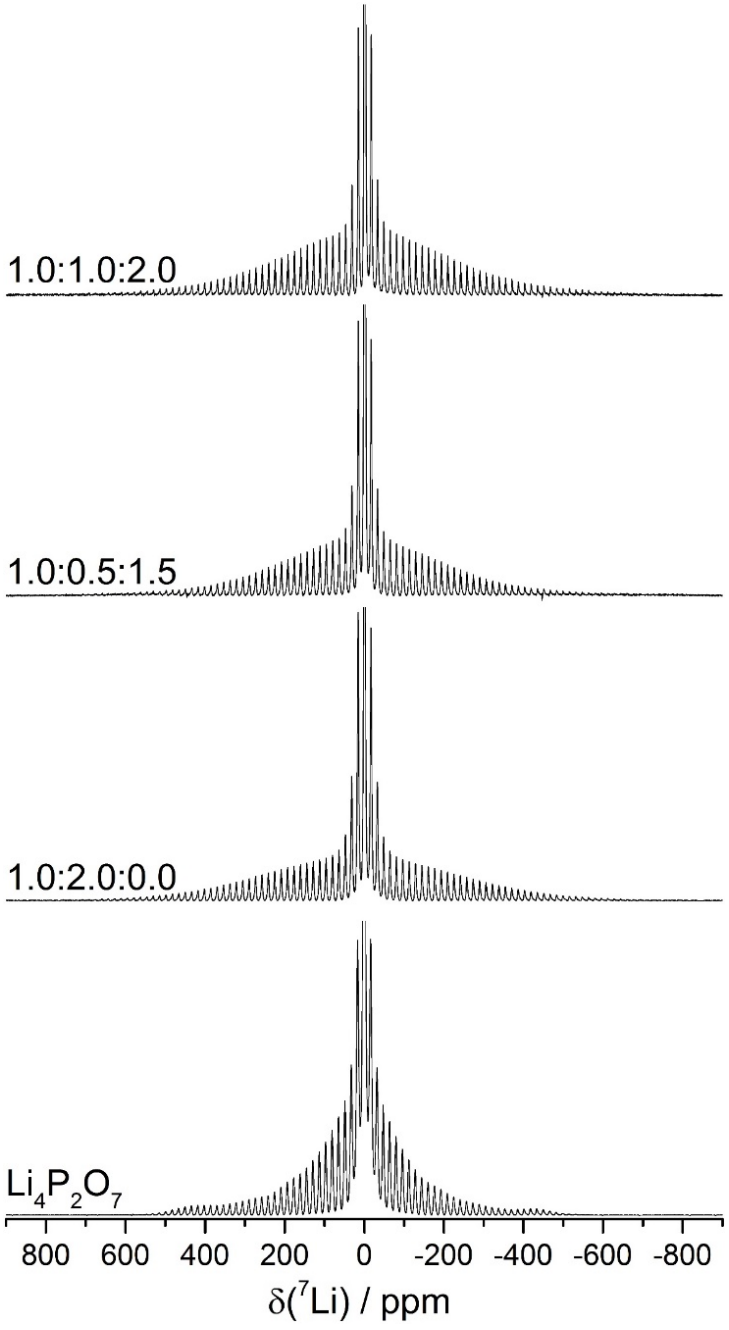

Figure 2: 155.5 MHz ^{7}Li MAS-NMR spectra of the glasses under study and the model compound $Li_4P_2O_7$. The central peak is off-scale. The spinning sideband pattern arises from the non-central Zeeman transitions.

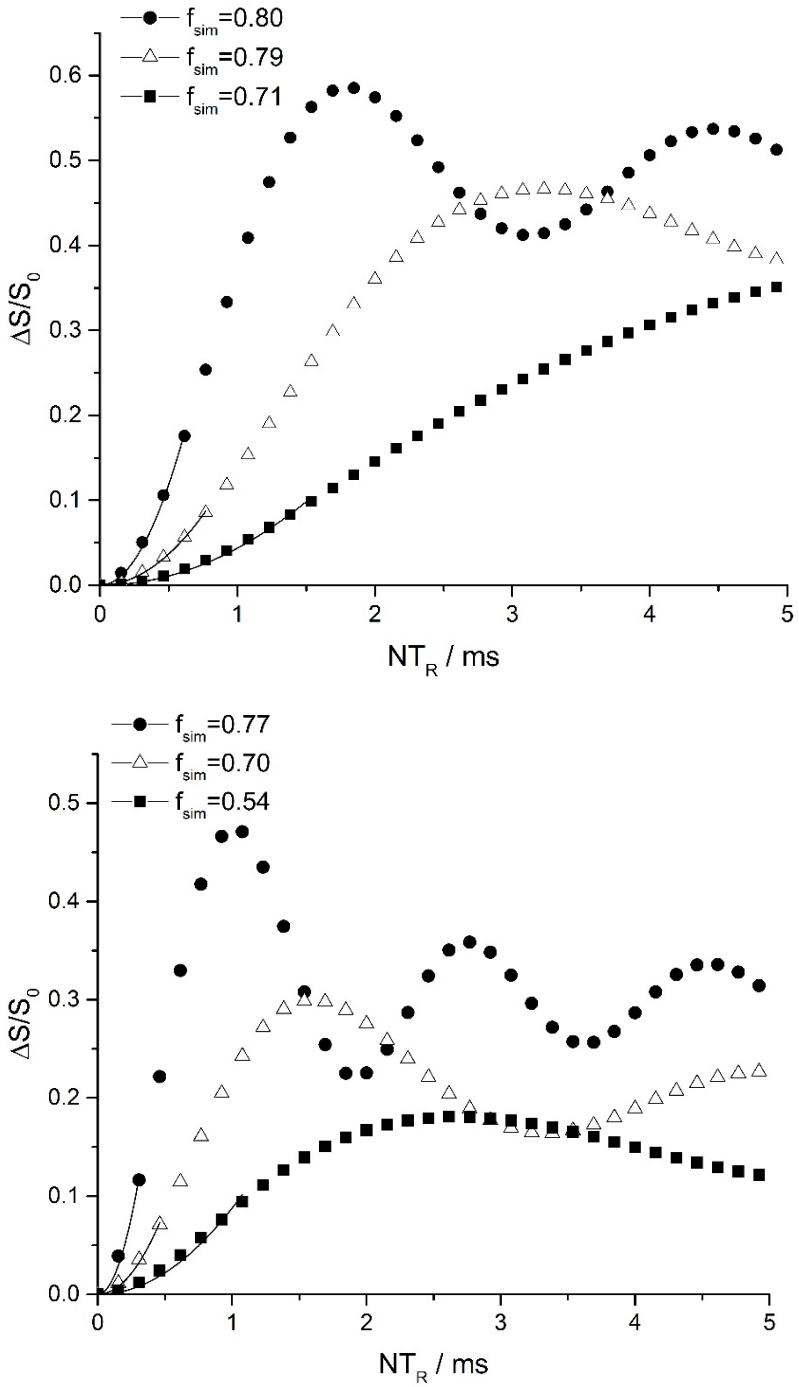

Figure 3. Top: Simulated $^{11}B\{^{6}Li\}$ REDOR curve for a two-spin system having an effective internuclear distance that is identical to that calculated from the multi-spin second moment M_2 (^{6}Li-^{11}B) of crystalline lithium diborate (black circles) and its approximation by a parabola. In addition, analogous simulations and their parabolic approximations are shown for dipolar coupling strengths of $0.3\times M_2$ (triangles) and $0.1\times M_2$ (squares). The corresponding values of f_{sim} applying to these three cases are listed as well. **Bottom**: Simulated $^{31}P\{^{6}Li\}$ REDOR curve for a two-spin system having an effective internuclear distance that is identical to that calculated from the second moment of crystalline $Li_4P_2O_7$ (black circles) and the approximation of the initial data range ($\Delta S/S_0 \leq 0.2$) by a parabola. In addition, analogous simulations and their parabolic approximations are shown for dipolar coupling strengths of $0.3\times M_2$ (triangles) and $0.1\times M_2$ (squares). The corresponding values of f_{sim} applying to these three cases are listed as well.

Application to the structural analysis of borophosphate glasses.

Armed with the experimental approach developed above, we are now in a position to characterize the relative strengths of ^{11}B- ^{6}Li and ^{31}P-^{6}Li magnetic dipole-dipole couplings in the two lithium borophosphate glasses. Before embarking on this, we present some basic structural characterization by Raman and MAS NMR spectroscopy in Figures 4 and 5. The Raman data of glasses B and C clearly reveal scattering frequencies near 1300 and 1160 cm^{-1}) which can be assigned to $P^{(3)}$ and $P^{(2)}$ units, respectively. In the $P^{(n)}$ terminology the superscript (n) specifies the number of bridging oxygen atoms to which the phosphorus species is bound; these bridging oxygen species are linked to other network former units (boron or phosphorus) in the glass structure. [32] Furthermore, the Raman band near 780 cm^{-1} can be attributed to the borate network [33]. This information is also consistent with the ^{31}P MAS-NMR spectra, which are poorly resolved owing to the extensive overlap of various species with different numbers of P-O-P versus P-O-B linkages. While in case of the glass B only a two-component deconvolution is justifiable, the deconvolution of the spectrum of glass C was previously suggested on the basis of numerous complementary advanced solid state NMR techniques sensitive to ^{31}P-^{31}P and ^{31}P-^{11}B spin-spin coupling [17], see Table 3. While these species represent different $P^{(n)}{}_{mB}$ species as discussed in reference [17] these deconvolution details are not relevant in the present study, as the ^{31}P{^{6}Li} REDOR analysis is done here on the dephasing of total ^{31}P NMR signal, representing the entire phosphorus inventory in this sample. The ^{11}B MAS-NMR spectra clearly differentiate between the different boron coordination states. The results of the spectral deconvolutions are summarized in Table 4. The two borophosphate glasses contain exclusively four-coordinated $B^{(4)}$ units, which give rise to well-defined sharp signals near -4.3 ppm. As previously discussed [17], the chemical shift indicates that these $B^{(4)}$ units are linked via bridging oxygens to four phosphorus atoms ($B^{(4)}{}_{4P}$ units). For glass B, the deconvolution reveals two such $B^{(4)}$ components. As discussed in more detail in reference [17], multiple $B^{(4)}$ peaks observed in such borophosphate glasses indicate species with different numbers of of B-O-P vs. B-O-B linkages. Thus, the signal observed near -3.4 ppm is assigned to $B^{(4)}$ species linked to fewer than four P atoms. In the lithium diborate glass D, the $B^{(4)}$ resonance is observed at 1.0 ppm ($B^{(4)}{}_{0P}$ units, exclusively B-O-B links). Furthermore large amounts of trigonal $B^{(3)}$ units (three bridging O atoms) are observed, in addition to some three-coordinate metaborate species carrying a non-bridging oxygen atom ($B^{(2)}$ units). These signals appear at higher chemical shift values (near 16 ppm) and their lineshapes are influenced by second-order quadrupolar perturbations.

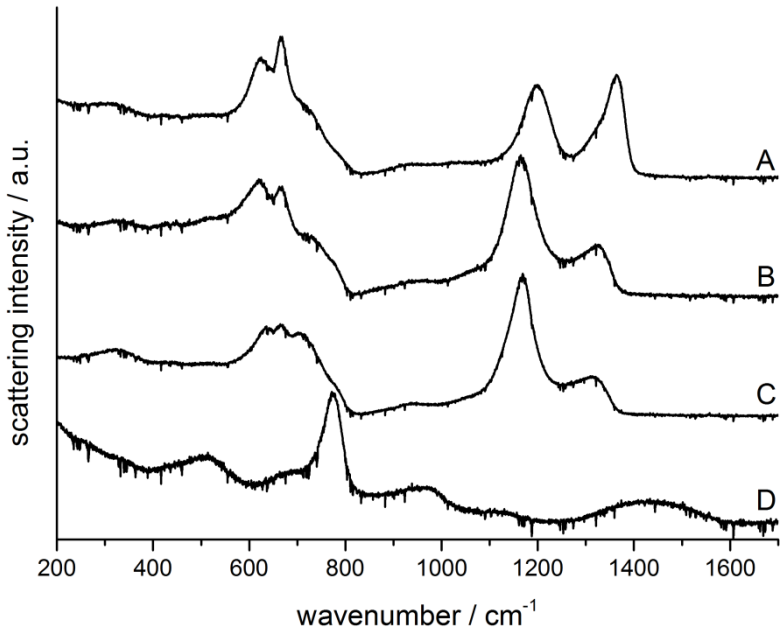

Figure 4. Raman scattering data obtained on the glasses under study. Glass A has the nominal composition $Li_2O:B_2O_3:P_2O_5$ = 1:1:4 and is prepared at the natural lithium isotopic abundance distribution. As substantial mass losses were observed during the synthesis of this glass (in agreement with a previous study of the Na-bearing system [18]), we refrained from synthesizing ^{6}Li isotopically enriched material for this composition.

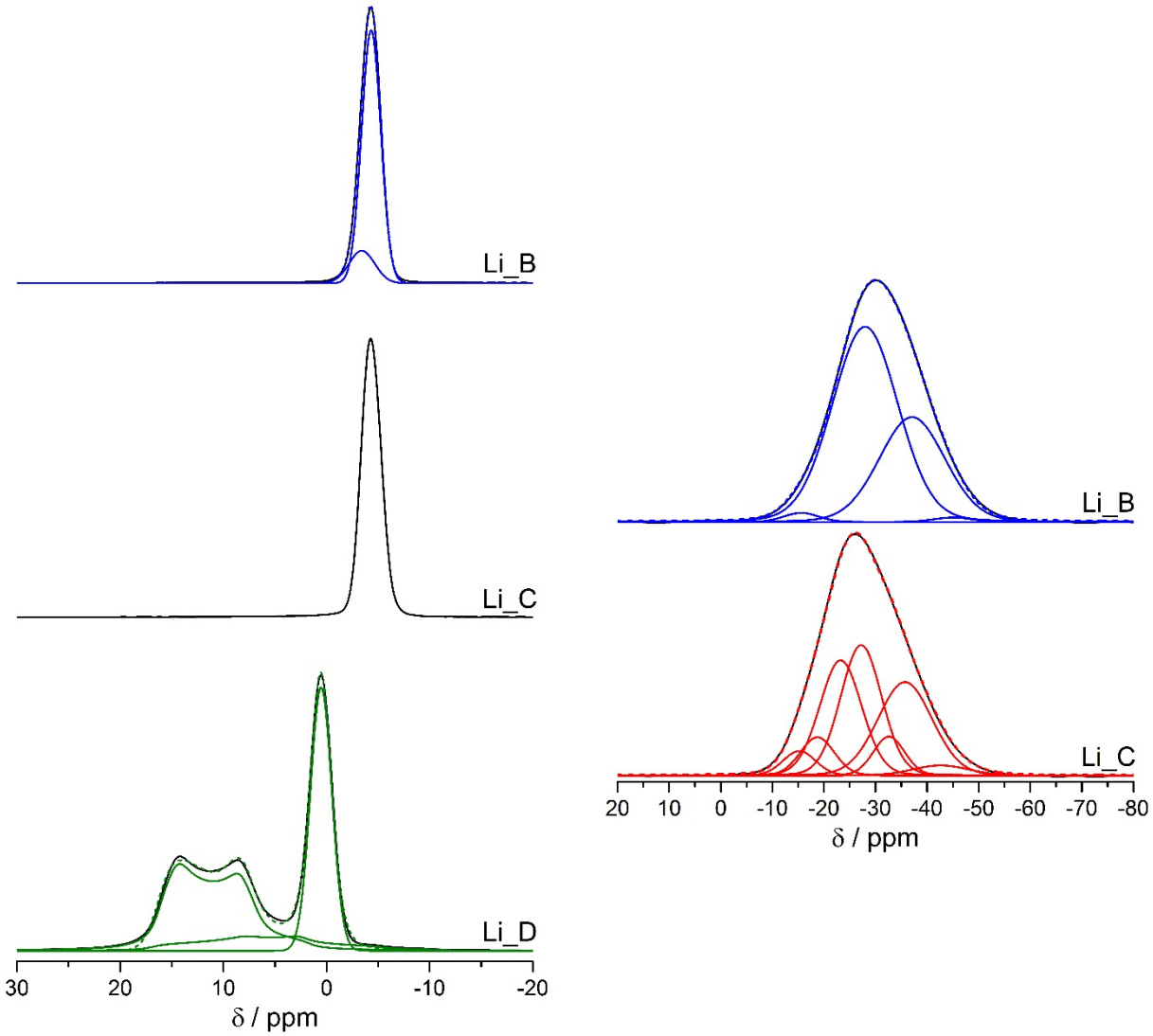

Figure 5: ^{11}B (left) and ^{31}P MAS-NMR (right) spectra of the investigated glasses, including peak deconvolutions. The deconvolution in the case of glass C is suggested based on previous complementary spectral editing experiments [17].

Figures 6 and 7 show the experimental ^{31}P{^{6}Li} and ^{11}B{^{6}Li} REDOR results on the samples under study. In the case of ^{31}P{^{6}Li} REDOR, the total integral of the ^{31}P signal was analyzed, whereas in the case of ^{11}B{^{6}Li} REDOR separate M_2 analyses were conducted for the B$^{(3)}$ and B$^{(4)}$ units in separate measurements. Application of equation (2) to the initial data range without any calibration factor would lead to the raw experimental M_{2raw} values, listed in Table 5. The results are compared to corresponding two-spin simulations (using the individual experimental conditions and quadrupole coupling parameters), which yield the best agreement with the experimental data within the data range $\Delta S/S_0 < 0.1$. (Note that in looking for best agreement, we focus on the initial data range, as the experimental data diverge from these two-spin

simulations over wider data ranges, because of the multi-spin character of the experimental samples studied here). The corresponding second moments obtained from these fits, $M_{2sim,}$ and the calibration factors f_{sim} defined by M_{2raw}/M_{2sim} are listed in Table 5. We note that the f_{sim} values for the glasses turn out to be significantly smaller than f_{sim} or f_{exp} for the crystalline model compounds. In the context of Figure 3 we attribute this finding to the much weaker dipolar coupling in the glasses. Thus, our results indicate that obtaining M_2 values by fitting experimental REDOR data to eq. (2), using calibration factors f_{exp} from model compound experiments, may lead to wrong results, if the dipolar coupling strengths in the model compounds are substantially different from those in the actual samples measured. Table 5 also lists the corresponding values of Σr_{IS}^{-6} calculated via eq. (3) from the M_{2sim} values for the three glasses studied, reflecting the effect of the distributions of the ^{6}Li nuclei around the ^{31}P and ^{11}B observe nuclei. This quantity allows a direct comparison of the data obtained from both ^{31}P{^{6}Li} REDOR and ^{11}B{^{6}Li} REDOR, as no nucleus-specific constants contribute to it. Table 5 indicates that for both borophosphate glasses the values of $\Sigma r_{B\text{-}Li}^{-6}$ relating to the B-Li distance distributions are significantly lower than the values of $\Sigma r_{P\text{-}Li}^{-6}$ relating to the P-Li distance distributions. This result clearly indicates that the phosphate species are (on average) significantly closer to the lithium ions than the borate species, despite the relatively low concentrations of anionic $P^{(2)}$ units in these glasses. This conclusion is further supported by the strikingly different $\Sigma r_{B\text{-}Li}^{-6}$ values measured in the lithium borophosphate glasses from the value measured for the lithium diborate glass, despite comparable lithium contents. The results obtained here confirm recent conclusions obtained for sodium borophosphate glasses, obtained by a comparison of ^{31}P{^{23}Na} and ^{11}B{^{23}Na} REDOR data. As a matter of fact, the respective numerical values of $\Sigma r_{P\text{-}Li}^{-6}$ and of $\Sigma r_{B\text{-}Li}^{-6}$ obtained here are found to be quite similar to the corresponding values $\Sigma r_{P\text{-}Na}^{-6}$ and $\Sigma r_{B\text{-}Na}^{-6}$ [18]. While in the case of the Na-borophosphate system the calibration factor was obtained empirically, without explicit consideration of the ^{23}Na nuclear electric quadrupole coupling constants, the approach delineated in the present study is more rigorous. Once again, our results confirm that - despite their formally uncharged status - the $P^{(3)}$ phosphate groups are the chief charge compensating species in alkali borophosphate glasses. The negative formal charge located on the $B^{(4)}_{4P}$ units is actually not found there, but it is dispersed into the network owing to the bond valence gradient encountered in the B-O-P linkages. As discussed previously [17,18] this mechanism leads to extensive charge re-distribution and delocalization, producing rather shallow Coulomb traps. This effect

is held responsible for the increased ionic mobility and ionic conductivity observed in comparison to pure alkali phosphate glasses.

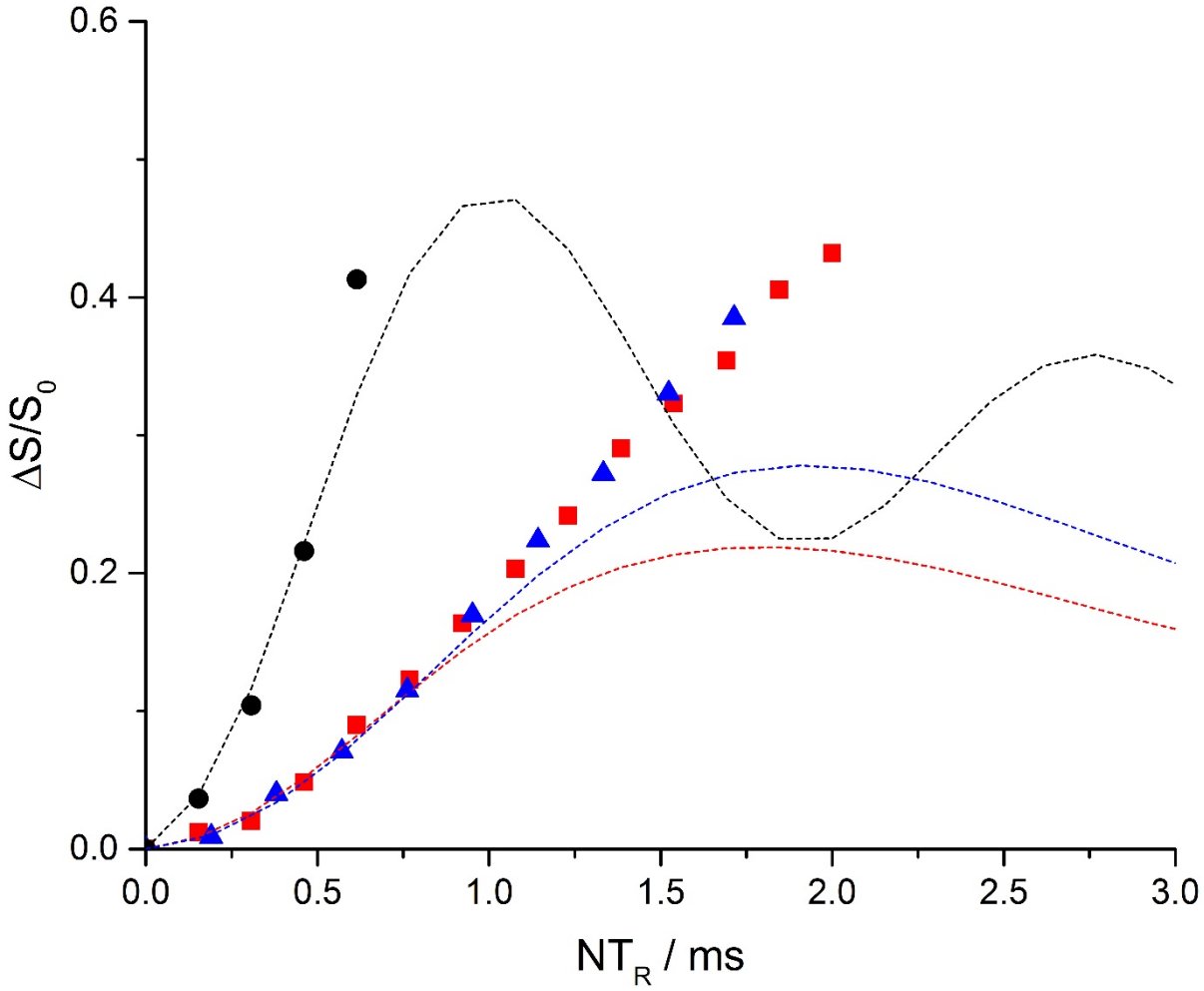

Figure 6: $^{31}P\{^{6}Li\}$ REDOR results on the lithium borophosphate glasses B (triangles) and C (squares) and the model compound $Li_4P_2O_7$ (circles). The total ^{31}P integral was analyzed, representing an average over all phosphorus sites. The results are compared to corresponding two-spin simulations (using the individual experimental conditions and quadrupole coupling parameters), producing the best agreement with the experimental data within the data range $\Delta S/S_0 \leq 0.1$. The corresponding M_{2sim} values and calibration factors f_{sim} are listed in Table 5.

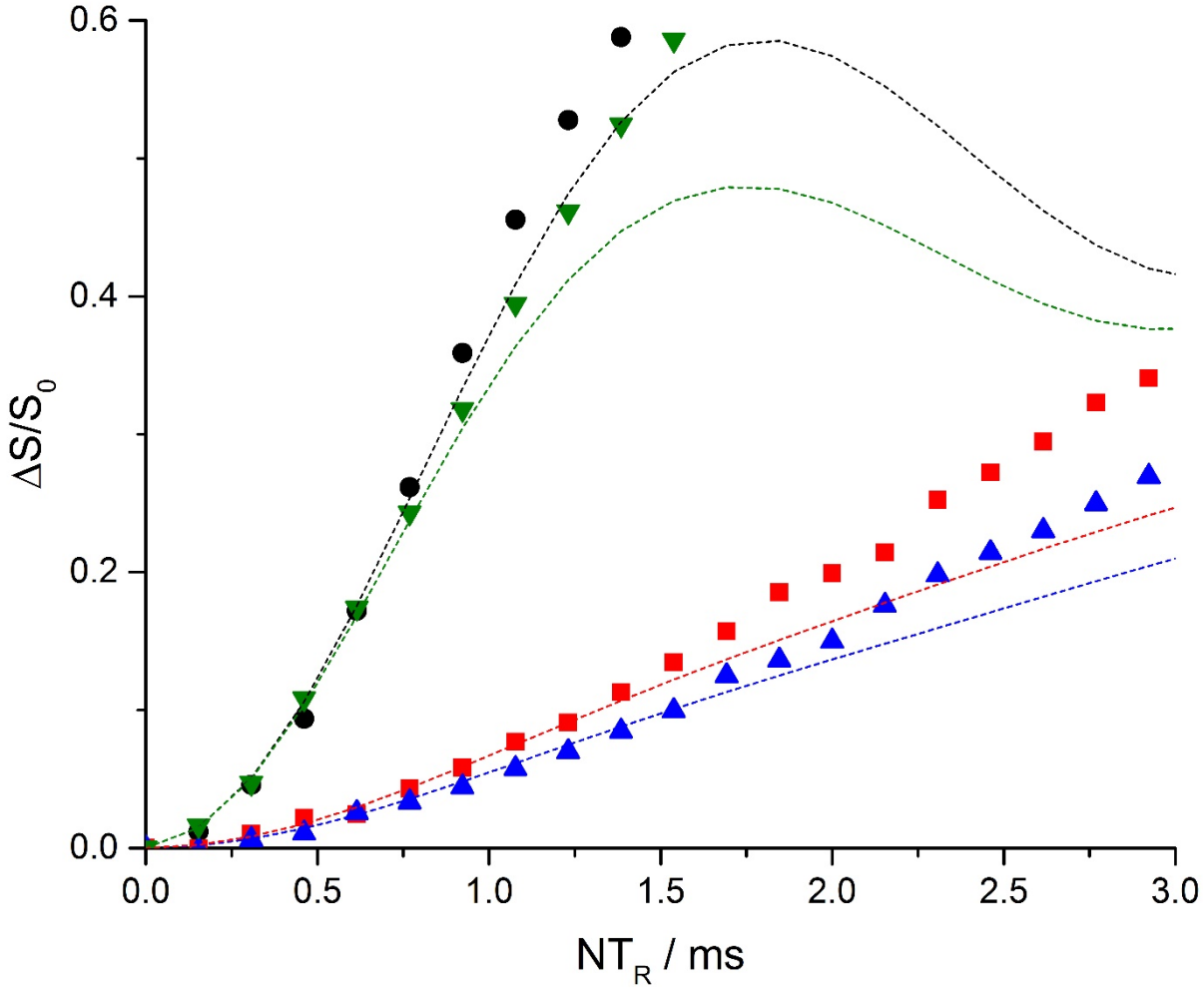

Figure 7: $^{11}B\{^{6}Li\}$ REDOR results on the lithium borophosphate glasses B (up-triangles), C (squares), D (down-triangles) and the model compound $Li_2B_4O_7$ (circles). The results are compared to corresponding two-spin simulations (using the individual experimental conditions and quadrupole coupling parameters), producing the best agreement with the experimental data within the data range $\Delta S/S_0 \leq 0.1$. The corresponding M_{2sim} values and calibration factors f_{sim} are listed in Table 5. In the case of the lithium diborate crystal and glass, results are shown for the four-coordinate ($B^{(4)}$) units.

Table 3: ^{31}P MAS-NMR spectral deconvolution, peak assignments and ^{31}P lineshape component parameters measured in the glasses: isotropic chemical shifts δ_{iso}, line broadening parameter Δ. In the $P^{(n)}_{mB}$ terminology, the superscript n denotes the number of bridging O atoms, while the subscript m denotes the number of B atoms to which the P atom is linked.

Composition		site	δ_{iso} / ppm ±0.5ppm	Δ/ppm ±0.1ppm	area /% ± 2 / %
B	1:1:2	$P^{(3)}_{0B}$	-44.0	15.0	1
		$P^{(3)}_{1B}$	-37.1	15.0	33
		$P^{(3)}_{2B}$	-28.0	15.0	64
		$P^{(3)}_{3B}$	-15.6	7.9	2
C	1:0.5:1.5	$P^{(3)}_{0B}$	-42.6	13.0	3
		$P^{(3)}_{1B}$	-35.7	12.5	27
		$P^{(2)}_{0B}$	-32.6	7.2	6
		$P^{(3)}_{2B}$	-27.2	9.4	28
		$P^{(2)}_{1B}$	-23.3	9.6	25
		$P^{(3)}_{3B}$	-18.7	7.8	7
		$P^{(2)}_{2B}$	-15.2	7.5	4

Table 4: Deconvolution of the ^{11}B MAS-NMR spectra and ^{11}B lineshape parameters measured in the glasses: isotropic chemical shifts δ_{iso}, line broadening parameter Δ, quadrupole coupling constant C_Q and asymmetry parameter η_Q. In the $B^{(n)}$ terminology, n specifies the number of bridging oxygen atoms bonded to B.

Composition		site	δ_{iso} / ppm	Δ/ppm	C_Q/MHz	η_Q	area /%
	$Li_2O:B_2O_3:P_2O_5$		±0.5ppm	±0.1ppm	±0.1MHz	±0.1	± 2%
B	1.0:1.0:2.0	$B^{(4)}$(1)	-4.3	2.2	-	-	88
		$B^{(4)}$(2)	-3.4	3.0	-	-	12
C	1.0:0.5:1.5	$B^{(4)}$	-4.3	2.3	-	-	100
D	1.0:2.0:0.0	$B^{(4)}$	0.2	2.5	-	-	38
		$B^{(3)}$	17.6	1.9	2.6	0.2	48
		$B^{(2)}$	17.0	2.1	3.3	0.6	14

Table 5 M_2 values (in units of 10^6 rad^{2}s^{-2}), experimental and simulated scaling factors, and distance sums $\Sigma r_{P\text{-}Li}^{-6}$ and $\Sigma r_{B\text{-}Li}^{-6}$ (in units of 10^{60}m^{-6} for the crystalline model compounds and the glasses.

Composition		site	M_2 theor.	M_{2raw}.	M_{2sim}.	f_{sim}	f_{exp}	Σr_{IS}^{-6}
	$Li_2O:B_2O_3:P_2O_5$			± 10%	±10%	± 0.02	± 10%	± 10%
B	1.0:1.0:2.0	$B^{(4)}$		0.29	0.60	0.48		0.0009
		P		1.44	2.02	0.71		0.0019
C	1.0:0.5:1.5	$B^{(4)}$		0.42	0.73	0.58		0.0011
		P		1.40	2.79	0.51		0.0026
D	1.0:2.0:0.0	$B^{(4)}$		3.51	4.58	0.77		0.0068
		$B^{(3)}$		3.22	4.18	0.77		0.0062
	$Li_2B_4O_7$	$B^{(4)}$	4.58	3.35	4.58	0.80	0.73	0.0068
		$B^{(3)}$	5.15	3.73	5.15	0.80	0.73	0.0076
	$Li_4P_2O_7$	$P^{(1)}$	12.10	8.83	12.60	0.70	0.73	0.0117

Conclusions

In summary, a simulation-based procedure has been developed for the analysis of REDOR experiments involving the interaction of spin-1/2 and spin-3/2 observe nuclei with multiple I = 1 spins, in terms of dipolar second moments, taking into account the nuclear electric quadrupolar interaction and the experimental measurement conditions. The simulations show that under conditions outside of the adiabatic limit the calibration factors to be applied to the analysis of experimental REDOR data via eq. (2) also depend on the strength of the dipolar coupling to be measured. This caveat needs to be kept in mind, when using experimental calibration procedures on the basis of crystalline model compound studies. In the present work, this procedure has been applied to probe the spatial proximity of ^{6}Li network modifier ions with the ^{11}B and ^{31}P nuclei in the amorphous framework of ion conducting lithium borophosphate glasses. The results indicate that the lithium ions are much closer to the (formally neutral) phosphate than to the (formally anionic) borate network component. As discussed elsewhere, this result, which can be understood in terms of bond valence concepts, also offers a structural rationale for the positive mixed-network former effect upon the electrical conductivity observed in alkali borophosphate glasses [17,18].

Acknowledgements

Authors acknowledge the Brazilian funding agencies FAPESP (CEPID Project 2013/07793-6) and CNPq (Universal Project 477053/2012-2 (HE). L.F. thanks the Foundation of German Business for a personal stipend.

References

(1) T. Gullion, J Schaefer, J. Magn. Reson. 81 (1989), 196.

(2) O. Toke, L. Cegelski, in *Solid State NMR Studies of Biomolecules*, A. McDermott, T. Polenova, eds., J. Wiley & sons 2010, p 473.

(3) T. Gullion, Ann. Rep. NMR Spectrosc. 65 (2009), 111.

(4) H. Eckert, S. Elbers, J. D. Epping, M. Janssen, M. Kalwei, W. Strojek, U. Voigt, Topics in Current Chemistry 246 (2005), 195.

(5) H. Eckert, Z. Phys. Chem.224 (2010), 1591.

(6) M. Bertmer, H. Eckert, H. Solid State Nucl. Magn. Reson. 15 (1999), 139.

(7) Z. Gan, Chem. Commun. (2006), 4712.

(8) L. Chen, X. Lu, Q. Wang, O. Lafon, J. Trebosc, F. Deng, J. P. Amoureux, J. Magn. Reson. 206 (2010), 269.
(9) X. Lu, O. Lafon, J. Trebosc, J. P. Amoureux, J. Magn. Reson. 215 (2011), 34.
(10) W. Strojek, M. Kalwei, H. Eckert, J. Phys. Chem. B 108 (2004), 7061.
(11) E.Nimerovsky, A. Goldbourt, Phys. Chem. Chem. Phys.14 (2012), 13437.
(12) E. Hughes, T. Gullion, A. Goldbourt, S. Vega, A.J. Vega, J. Magn. Reson. 156 (2002), 230.
(13) A.Schmidt, J. S. Schaefer, J. Magn. Reson. 96 (1992), 644.
(14) R. Böhmer, K. R: Jeffrey, M. Vogel, Prog. NMR Spectrosc. 50 (2007), 87.
(15) S. Faske, H. Eckert, M. Vogel, Phys. Rev. B 77 (2008), 104301.
(16) S. Puls, H. Eckert, Phys. Chem. Chem. Phys. 9 (2007), 3992.
(17) D. Larink, H. Eckert, M. Reichert, S. W. Martin, J. Phys. Chem. C 116 (2012), 26162.
(18) L. Funke, H. Eckert J. Phys. Chem. C. 120 (2016), 3196.
(19) L. van Wüllen, H. Eckert, G. Schwering, Chem. Mater., 12 (2000), 1840.
(20) D. Massiot, F. Fayon, M. Capron, I. King, S. L. Calve, B. Alonso, J. O. Durand, B. Bujoli,, Z. Gan, G. Hoatson, Magn. Reson. Chem. 40 (2002) 70..
(21) J. R. Garbow, T. Gullion, J. Magn. Reson. 95 (1991), 442.
(22) M. Bak, J. T. Rasmussen, N.C. Nielsen, J. Magn. Reson. 147 (2000), 296.
(23) J. H. van Vleck, Phys. Rev. 74 (1948), 1168.
(24) T. Hasiuk, K. R. Jeffrey, Solid State Nucl. Magn. Reson. 34 (2008), 228.
(25) B. Gee, H. Eckert, Ber. Bunsenges. Phys. Chem.100 (1996), 1610.
(26) N. J. Stone, Atomic Data and Nuclear Tables 111-112 (2016), 1.
(27) D. Freude, J. Haase, NMR-Basic Principles and Progress 29 (1993), 1.
(28) N. K. Sung, S. Ho, A. R. Lim, J. N. Kim, Sae Mulli 35 (1995), 670.
(29) Y. N. Ivanov, Y. V. Burak, K. S. Aleksandrov, Sov. Phys. Solid State 32 (1990), 1955.
(30) A. Senyshyn, H. Fuess, H. Boysen, R. Niewa, J., Banys, M. Kinka, Y. V. Burak, V. T. Adamiv, F. Izumi, I. V. Chumak, J. Phys. D 45 (2012), 1.
(31) A. Daidouh, M. L. Veiga, C. Pico, M. Martinez-Ripol, Acta Crystallogr. C 53 (1997), 167.
(32) J. J. Hudgens, R. K. Brow, D. R. Tallant, S. W. Martin, J. Non-Cryst. Solids 223 (1998), 21.
(33). W. L. Konijendijk, J. M. Stevels, J. Non-Cryst. Solids 18 (1975), 307.